PNAS

Supporting Information for

Lanthanide Binding Peptide Surfactants at Air-Aqueous Interfaces for Interfacial Separation of Rare Earth Elements

Luis E. Ortuno Macias[1], Felipe Jiménez-Ángeles[2], Jason G. Marmorstein[3], Yiming Wang[4], Stephen A. Crane[4], Surabh KT[1], Pan Sun[5], Bikash Sapkota[5], Eshe Hummingbird[3], Woojin Jung[4], Baofu Qiao[2], Daeyeon Lee[4], Ivan J. Dmochowski[3], Robert Messinger[1], Mark L. Schlossman[5], Ravi Radhakrishnan[4], E. James Petersson[3], Monica Olvera de la Cruz[2], Wei Bu[6], Mrinal Bera[6], Binhua Lin[6], Raymond Tu[1], Kathleen J. Stebe[4*], Charles Maldarelli[1*].

[1]Department of Chemical Engineering, The City College of New York, New York, 10031, New York, USA.
[2]Department of Materials Science and Engineering, Northwestern University, Evanston, 60208, Illinois, USA.
[3]Department of Chemistry, University of Pennsylvania, Philadelphia, 19104, Pennsylvania, USA.
[4]Department of Chemical and Biomolecular Engineering, University of Pennsylvania, Philadelphia, 19104, Pennsylvania, USA.
[5]Department of Physics, University of Illinois at Chicago, Chicago, 60607, Illinois, USA.
[6]NSF's ChemMatCARS, Pritzker School of Molecular Engineering, University of Chicago, Chicago, 60637, Illinois, USA.

[*]Corresponding authors: Kathleen J. Stebe, Charles Maldarelli.
[*]Email: kstebe@seas.upenn.edu, cmaldarelli@ccny.cuny.edu.

This PDF file includes:

Free energy calculations from MD simulations.
The change of the free energy is calculated using the slow-growth method in thermodynamic integration to transform the system from state A to state B as follows(1-3):

$$G^B(T,p) - G^A(T,p) = \int_0^l \langle \frac{\partial H}{\partial \lambda} \rangle_\lambda d\lambda \qquad (S1)$$

l is a coupling parameter that varies from 0 to 1 to modulate the interaction between the target molecule and the medium that is gradually turned in the system's Hamiltonian, such that the interaction between the medium and the molecule is switched off at state A (l=0) and is on in state B (l =0), H is the Hamiltonian that contains the interactions between all the atoms in the system, and λ is a coupling parameter employed to turn on and off the interactions of the molecule by varying it from 0 to 1.

$$\Delta G = \int_0^1 \left\langle \frac{\partial H}{\partial \lambda} \right\rangle_\lambda d\lambda \qquad (S2)$$

Surface concentration of molecules at interface.
From the corresponding fitting of the XR data, values such as electron density, thickness, and interfacial roughness (Supplementary Tables 2-7) can be obtained. These parameters allowed us to compute surface concentration of peptide adsorbed to the air-water interface for each LBTs and LBTs/Tb^{3+} adsorbed layers to the air-aqueous interface from bulk solution. To compute the surface concentrations of molecules populating the air water interface we applied electron density and molar volume balances resulting in:

$$e_T = \Gamma_{LBTs} e_{LBTs} + \Gamma_{Tb^{3+}} e_{Tb^{3+}} + \Gamma_w e_w \qquad (S3)$$

$$d_T = \Gamma_{LBTs} V_{LBTs} + \Gamma_{Tb^{3+}} V_{Tb^{3+}} + \Gamma_w V_w \qquad (S4)$$

with,

- d_T (Å) is the total thickness of the layer:

$$d_T = \sum d_i = d_1 + d_2 \qquad (S5)$$

Note that the total thickness of the layer varies for different samples, depending on the coordination state (bound or unbound), peptide, and bulk concentration of peptide. For all uncomplexed peptides, the total thickness of the layer ranges between 26 Å and 37 Å. This total thickness (interfacial layer) is generally reduced in the complexed state, as the peptide transitions from an open state to a closely packed conformation. However, a larger total thickness is observed for the highest concentration of $LBTLLA^{5-}$ at a peptide:Tb^{3+} ratio of 4, potentially due to a higher amount of peptide adsorbed under these concentrated conditions.
Other variations, such as a larger thickness for the lower concentration of LBT^{3-}:Tb^{3+} compared to the middle and larger concentrations, might result from a more populated interface leading to a more packed conformation of complexes. In general, changes in thickness from sample to sample are also accompanied by changes in electron density (reduction in electron density of one of the slabs constituting the entire layer), indicating structural conformational changes of the peptide or peptide-metal complex. These variations will not impact the calculations, as they are based on the sum of the thicknesses of all slabs and the sum of the electron density values from each slab.

- e_T (electrons/Å^2) is the electron surface density of the air-water interface:

$$e_T = \sum d_i \rho_i = d_1 \rho_1 + d_2 \rho_2 \qquad (S6)$$

- e_w is the number of electrons in a water molecule (10 e/molecule).
- V_W is the molar volume of water molecules (30 Å^3/molecule).
- $e_{Tb^{3+}}$ is the number of electrons in a Terbium cation (62 electrons/ion).
- $V_{Tb^{3+}}$ is the partial molar volume of Tb^{3+} ions, calculated from the ionic radius in standard tables and with a value of approximately 5.43 Å^3/ion(4).
- e_{LBTs} is the number of electrons in each LBT peptide molecule (LBT^{5-}: 1054 electrons/molecule, LBT^{3-}: 1052 electrons/molecule, and $LBTLLA^{5-}$: 1216 electrons/molecule).
- V_{LBTs} is the partial molar volume of each LBT peptide calculated from MD simulations (LBT^{5-}: 2.214 $\pm$ 0.005 nm^3, $LBTLLA^{5-}$: 2.671 $\pm$ 0.002 nm^3, and LBT^{3-}: 2.361 $\pm$ 0.004 nm^3).
- Γ_{LBTs} and Γ_W are the surface concentration (molecules/ Å^2) of LBT peptide and water respectively (both unknown).
- $\Gamma_{Tb^{3+}}$ is the surface concentration of Tb^{3+} ions obtained from the x-ray fluorescence near total reflection (XFNTR) analysis (see below).

Interfacial water can be divided into water outside of the binding loop and retained in the binding loop; Γ_W refers to water outside of the loop. A water molecule present inside of the loop would contribute negligibly to the sum of the electrons per peptide.

Origins of differences in dissociation constants between values reported in this work and prior studies.

The Nitz *et al.* peptide with an amide at the C terminus is uncharged while LBT^{5-}, with a carboxylic group, is disassociated at pH 6 since the pK_a of the C terminus for folded proteins is on average 3.3(5). This additional terminal charge can sterically hinder the coordination site by altering the hydrophobic cluster formed between the amino acids near the C- and N- terminus, which is fundamental for the high affinity of the molecule for Tb^{3+} as noted by Nitz *et al.* (see also Fig. 4a for this interaction in LBT^{5-}) and therefore can account for the increase in K_D. The differing values of pH affects the ionization of the carboxylic groups of the aspartic acid (D) and glutamic acid (E) residues that coordinate as Lewis bases with the Tb^{3+} in the binding pocket; the lower pH of our measurements can result in partial protonation which would reduce the affinity and increase K_D. In this regard it is important to note that while the average pK_A for D and E are 4.2 and 3.5, two units below our pH of 6. However, these pK_As are perturbed and are generally larger in clusters of negative charge as in the environment in the binding loop (deprotonation of the –COOH becomes more difficult with excess surrounding negative charge). Hence partial protonation of these groups can be expected at our pH of 6. Finally, the average value of the pK_A of the N terminus for folded proteins in 7.7(5) and hence this group will be more significantly protonated at pH 6 than 7, with the additional charge affecting the ability of the loop to wrap around the cation; note the proximity of the N terminus to the binding loop chelators in Fig. 4a. Additionally, the buffer concentrations in our experiment are much larger than in Nitz *et al.* (50 mM compared to 10 mM) and this difference

could influence electrostatic interactions between the charged peptide side chains in the loop and the cations by reducing electrostatic attractions through charge shielding.

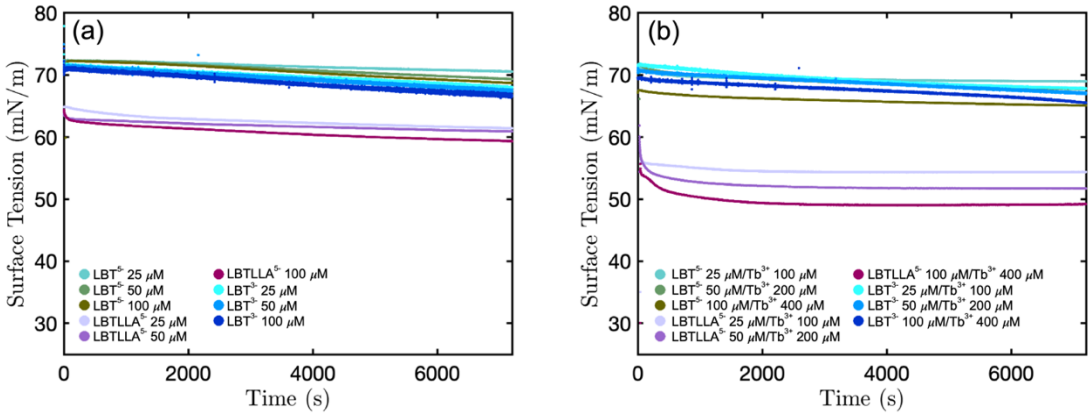

Fig. S1. Dynamic surface tension relaxation measurements for (a) solutions containing LBT^{5-}, $LBTLLA^{5-}$, and LBT^{3-} at different bulk concentrations, and (b) solutions containing LBT^{5-}/Tb^{3+}, $LBTLLA^{5-}/Tb^{3+}$, and LBT^{3-}/Tb^{3+} at different bulk concentrations.

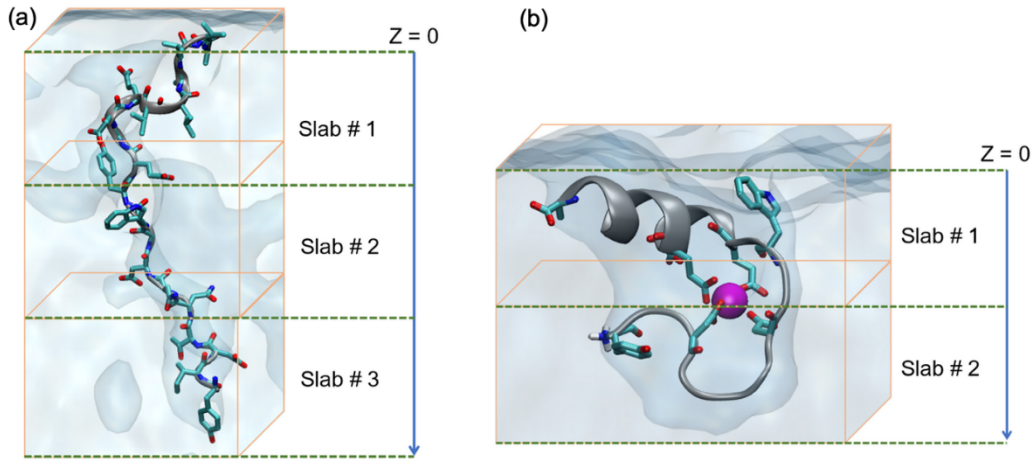

Fig. S2. Schematic illustration of the 2- and 3-slab model used to fit the reflectivity data for LBTs and LBTs:Tb^{3+} at the air water interface, where (a) represents an uncomplexed extended LBT peptide and (b) represents a Ln^{3+}-LBT complex. (a) LBT^{5-} at the air-aqueous interface, and (b) $LBTLLA^{5-}/Tb3^{+}$ complex at the air-aqueous interface.

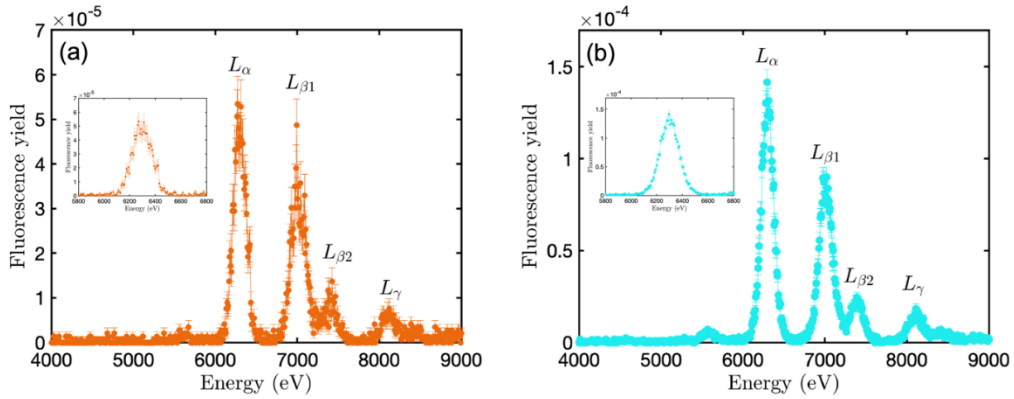

Fig. S3. Normalized fluorescence spectra from the samples containing Tb^{3+} cations at $Q_Z = 0.021$ Å^{-1} with the $\mathcal{L}_\alpha$, $\mathcal{L}_{\beta1}$, $\mathcal{L}_{\beta2}$, and $\mathcal{L}_\gamma$ fluorescence peaks of Tb^{3+}. (a) Normalized fluorescence spectra from the reference sample containing 25 mM of Tb^{3+}. (b) Integrated fluorescence spectra from the samples containing 100 μM of Tb^{3+} and peptide. $\mathcal{L}_\alpha$ fluorescence peak or terbium was fit to a Gaussian function over the energy range from 5900 eV to 6700 eV (shown in the inset plots) to obtain its integrated area, which provides the XFNTR signal. The details of this calculation are described somewhere else(6-7).

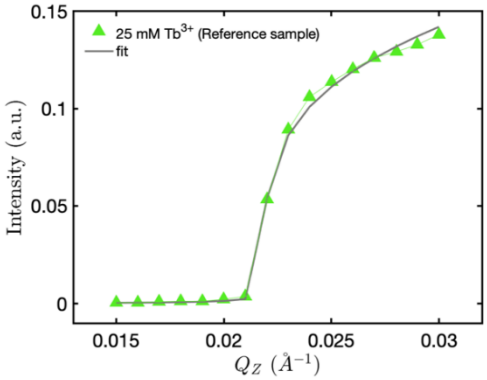

Fig. S4. Integrated fluorescence intensity from Tb^{3+} $\mathcal{L}_\alpha$ for a reference sample (buffer solution containing 25 mM of $TbCl_3$). The greater intensity at high Q_Z indicates that the bulk contribution dominates the signal. The fluorescence integration, and further XFNTR fitting for the reference samples was done to obtain a scale factor determined by the scattering geometry and elements, which are necessary to obtain the interfacial coverage of Tb^{3+} cations at the air/water interface.

Table S1. Fitting parameters from XR measurements from adsorbed layers of solutions containing LBT^{5-}, $LBTLLA^{5-}$, or LBT^{3-} at different bulk concentrations.*

	LBT^{5-} 25 μM			**LBT^{5-} 50 μM**			**LBT^{5-} 100 μM**		
Slab #	$\boldsymbol{d}$ (Å)	$\boldsymbol{\rho}$ $(e^-/Å^3)$	$\boldsymbol{\sigma}$ (Å)	$\boldsymbol{d}$ (Å)	$\boldsymbol{\rho}$ $(e^-/Å^3)$	$\boldsymbol{\sigma}$ (Å)	$\boldsymbol{d}$ (Å)	$\boldsymbol{\rho}$ $(e^-/Å^3)$	$\boldsymbol{\sigma}$ (Å)
1	$11.8^{\pm0.1}$	$0.3551^{\pm0.0003}$	$2.575^{\pm0.005}$	$10.8^{\pm0.3}$	$0.370^{\pm0.001}$	$2.82^{\pm0.02}$	$10.6^{\pm0.4}$	$0.371^{\pm0.002}$	$2.49^{\pm0.02}$
2	$10.9^{\pm0.5}$	$0.3373^{\pm0.0002}$	$2.575^{\pm0.005}$	$9.4^{\pm0.5}$	$0.3391^{\pm0.0004}$	$2.82^{\pm0.02}$	$9.1^{\pm0.3}$	$0.343^{\pm0.001}$	$2.49^{\pm0.02}$
3	$14.9^{\pm0.6}$	$0.3349^{\pm0.0002}$	$2.575^{\pm0.005}$	$12.0^{\pm0.4}$	$0.3345^{\pm0.0001}$	$2.82^{\pm0.02}$	$10.4^{\pm0.6}$	$0.3360^{\pm0.0005}$	$2.49^{\pm0.02}$
	$LBTLLA^{5-}$ 25 μM			**$LBTLLA^{5-}$ 50 μM**			**$LBTLLA^{5-}$ 100 μM**		
Slab #	$\boldsymbol{d}$ (Å)	$\boldsymbol{\rho}$ $(e^-/Å^3)$	$\boldsymbol{\sigma}$ (Å)	$\boldsymbol{d}$ (Å)	$\boldsymbol{\rho}$ $(e^-/Å^3)$	$\boldsymbol{\sigma}$ (Å)	$\boldsymbol{d}$ (Å)	$\boldsymbol{\rho}$ $(e^-/Å^3)$	$\boldsymbol{\sigma}$ (Å)
1	$10.8^{\pm0.1}$	$0.3985^{\pm0.0007}$	$2.42^{\pm0.01}$	$9.9^{\pm0.4}$	$0.404^{\pm0.008}$	$2.69^{\pm0.09}$	$10.8^{\pm0.2}$	$0.402^{\pm0.001}$	$2.65^{\pm0.02}$
2	$8.4^{\pm0.1}$	$0.3438^{\pm0.0004}$	$2.42^{\pm0.01}$	$7.3^{\pm0.2}$	$0.349^{\pm0.003}$	$2.69^{\pm0.09}$	$7.8^{\pm0.1}$	$0.3476^{\pm0.0009}$	$2.65^{\pm0.02}$
3	$12.9^{\pm0.4}$	$0.3348^{\pm0.0001}$	$2.42^{\pm0.01}$	$11.9^{\pm0.7}$	$0.3356^{\pm0.0004}$	$2.69^{\pm0.09}$	$12.7^{\pm0.3}$	$0.3352^{\pm0.0001}$	$2.65^{\pm0.02}$
	LBT^{3-} 25 μM			**LBT^{3-} 50 μM**			**LBT^{3-} 100 μM**		
Slab #	$\boldsymbol{d}$ (Å)	$\boldsymbol{\rho}$ $(e^-/Å^3)$	$\boldsymbol{\sigma}$ (Å)	$\boldsymbol{d}$ (Å)	$\boldsymbol{\rho}$ $(e^-/Å^3)$	$\boldsymbol{\sigma}$ (Å)	$\boldsymbol{d}$ (Å)	$\boldsymbol{\rho}$ $(e^-/Å^3)$	$\boldsymbol{\sigma}$ (Å)
1	$2.4^{\pm0.4}$	$0.20^{\pm0.04}$	$2.9^{\pm0.1}$	$4.7^{\pm0.2}$	$0.25^{\pm0.01}$	$2.96^{\pm0.07}$	$5.62^{\pm0.04}$	$0.263^{\pm0.002}$	$2.92^{\pm0.02}$
2	$10.7^{\pm0.3}$	$0.384^{\pm0.002}$	$2.9^{\pm0.1}$	$13.5^{\pm0.4}$	$0.3862^{\pm0.0007}$	$2.96^{\pm0.07}$	$14.8^{\pm0.1}$	$0.4014^{\pm0.0004}$	$2.92^{\pm0.02}$
3	$13.0^{\pm0.2}$	$0.\ 341^{\pm0.0003}$	$2.9^{\pm0.1}$	$9.8^{\pm0.2}$	$0.3445^{\pm0.0005}$	$2.96^{\pm0.07}$	$9.33^{\pm0.08}$	$0.3511^{\pm0.0003}$	$2.92^{\pm0.02}$

*Parameters: $\boldsymbol{d}$ is the layer thickness, $\boldsymbol{\rho}$ is the density, and $\boldsymbol{\sigma}$ is the interfacial roughness. Errors in the fitted parameters are obtained by mapping the chi-squared space.

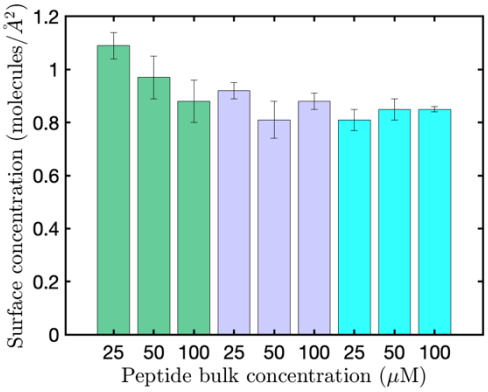

Fig. S5. Interfacial concentration of water molecules from surface layers of LBT^{5-}, $LBTLLA^{5-}$, and LBT^{3-} as a function of peptide bulk concentration.

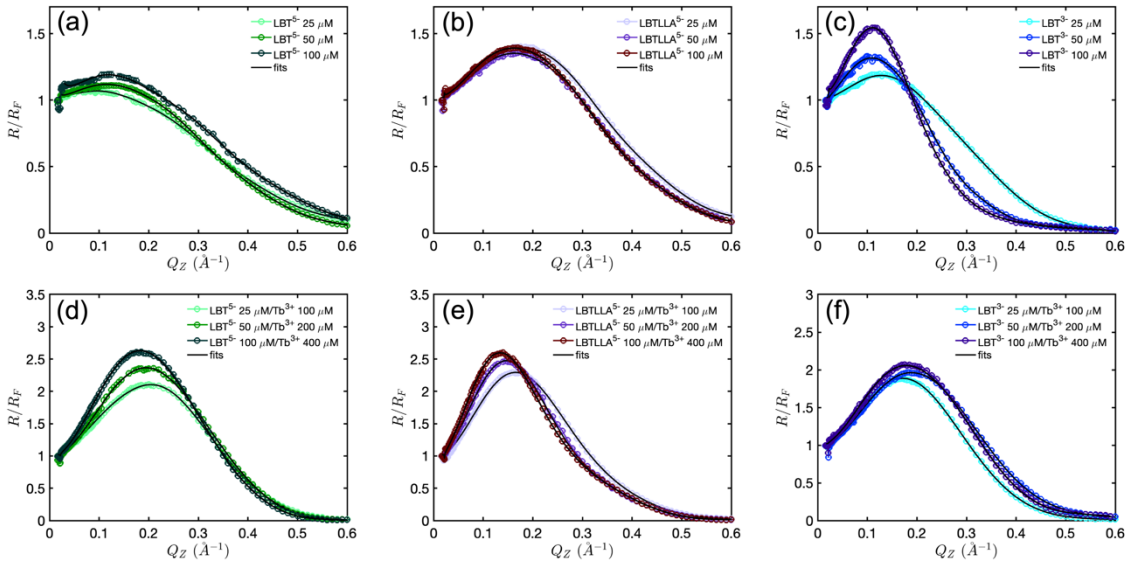

Fig. S6. Normalized reflectivity ($\mathcal{R}/\mathcal{R}_\mathcal{F}$) as a function of Q_Z normal to the surface for interfacial layers of LBT^{5-}, $LBTLLA^{5-}$, and LBT^{3-} at the air-water interface from solutions of 25, 50, and 100 μM LBT without Ln^{3+} cations (a, b, c) and with Tb^{3+} cations (d, e, f) in a 1:4 ratio of LBT to Tb^{3+}. Error bars, from the statistical uncertainty arising from counting photons, are plotted but are too small to be visible.

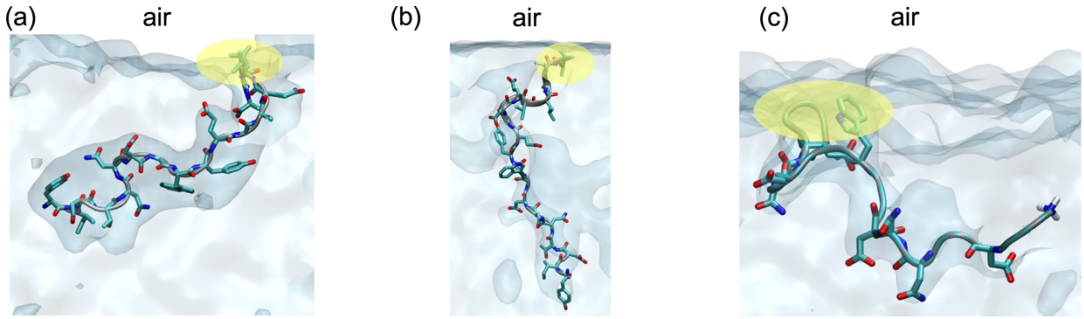

Fig. S7. MD simulations of single LBT molecules adsorbing to the interface (a) LBT^{5-}, (b) $LBTLLA^{5}$, and (c) LBT^{3-}.Yellow circles are used to highlight the residues close to the air phase at the surface.

Table S2. Fitting parameters from XR measurements from adsorbed layers of solutions containing LBT^{5-}/Tb^{3+}, $LBTLLA^{5-}/Tb^{3+}$, or LBT^{3-}/Tb^{3+} at different bulk concentrations. *

	LBT^{5-} 25 μM/Tb^{3+} 100 μM			**LBT^{5-} 50 μM/Tb^{3+} 200 μM**			**LBT^{5-} 100 μM/Tb^{3+} 400 μM**		
Slab #	d (Å)	ρ ($e^-/Å^3$)	σ (Å)	d (Å)	ρ ($e^-/Å^3$)	σ (Å)	d (Å)	ρ ($e^-/Å^3$)	σ (Å)
1	$10.07^{\pm0.07}$	$0.504^{\pm0.002}$	$3.34^{\pm0.02}$	$10.3^{\pm0.1}$	$0.545^{\pm0.005}$	$3.44^{\pm0.03}$	$10.0^{\pm0.3}$	$0.58^{\pm0.01}$	$3.81^{\pm0.09}$
2	$15.9^{\pm0.3}$	$0.3337^{\pm0.0002}$	$3.34^{\pm0.02}$	$14.3^{\pm0.3}$	$0.340^{\pm0.001}$	$3.44^{\pm0.03}$	$13.4^{\pm093}$	$0.3389^{\pm0.0007}$	$3.81^{\pm0.09}$
	$LBTLLA^{5-}$ 25 μM/Tb^{3+} 100 μM			**$LBTLLA^{5-}$ 50 μM/Tb^{3+} 200 μM**			**$LBTLLA^{5-}$ 100 μM/Tb^{3+} 400 μM**		
Slab #	d (Å)	ρ ($e^-/Å^3$)	σ (Å)	d (Å)	ρ ($e^-/Å^3$)	σ (Å)	d (Å)	ρ ($e^-/Å^3$)	σ (Å)
1	$11.81^{\pm0.06}$	$0.4909^{\pm0.0009}$	$3.26^{\pm0.01}$	$12.59^{\pm0.06}$	$0.4953^{\pm0.0007}$	$3.45^{\pm0.01}$	$11.8^{\pm0.2}$	$0.513^{\pm0.002}$	$3.63^{\pm0.03}$
2	$8.53^{\pm0.04}$	$0.3669^{\pm0.0005}$	$3.26^{\pm0.01}$	$9.02^{\pm0.03}$	$0.3868^{\pm0.0006}$	$3.45^{\pm0.01}$	$9.70^{\pm0.07}$	$0.407^{\pm0.001}$	$3.63^{\pm0.03}$
3	---	---	---	---	---	---	$8.2^{\pm0.3}$	$0.3421^{\pm0.0007}$	$3.63^{\pm0.03}$
	LBT^{3-} 25 μM/Tb^{3+} 100 μM			**LBT^{3-} 50 μM/Tb^{3+} 200 μM**			**LBT^{3-} 100 μM/Tb^{3+} 400 μM**		
Slab #	d (Å)	ρ ($e^-/Å^3$)	σ (Å)	d (Å)	ρ ($e^-/Å^3$)	σ (Å)	d (Å)	ρ ($e^-/Å^3$)	σ (Å)
1	$11.72^{\pm0.03}$	$0.4687^{\pm0.0008}$	$3.51^{\pm0.01}$	$8.7^{\pm0.2}$	$0.524^{\pm0.007}$	$3.59^{\pm0.04}$	$9.2^{\pm0.2}$	$0.512^{\pm0.003}$	$3.55^{\pm0.02}$
2	$9.3^{\pm0.3}$	$0.3386^{\pm0.0003}$	$3.51^{\pm0.01}$	$6.5^{\pm0.3}$	$0.346^{\pm0.002}$	$3.59^{\pm0.04}$	$4.87^{\pm0.09}$	$0.376^{\pm0.004}$	$3.55^{\pm0.02}$

*Parameters: d is the layer thickness, ρ is the density, and σ is the interfacial roughness. Errors in the fitted parameters are obtained by mapping the chi-squared space.

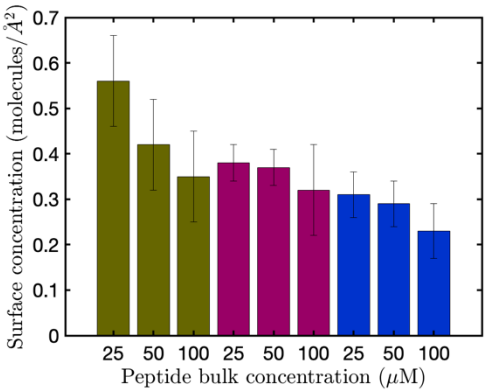

Fig. S8. Interfacial concentration of water molecules from surface layers of LBT^{5-}, $LBTLLA^{5-}$, and LBT^{3-} as a function of peptide bulk concentration with Tb^{3+} cations at a ratio LBT:Tb^{3+} of 1:4.

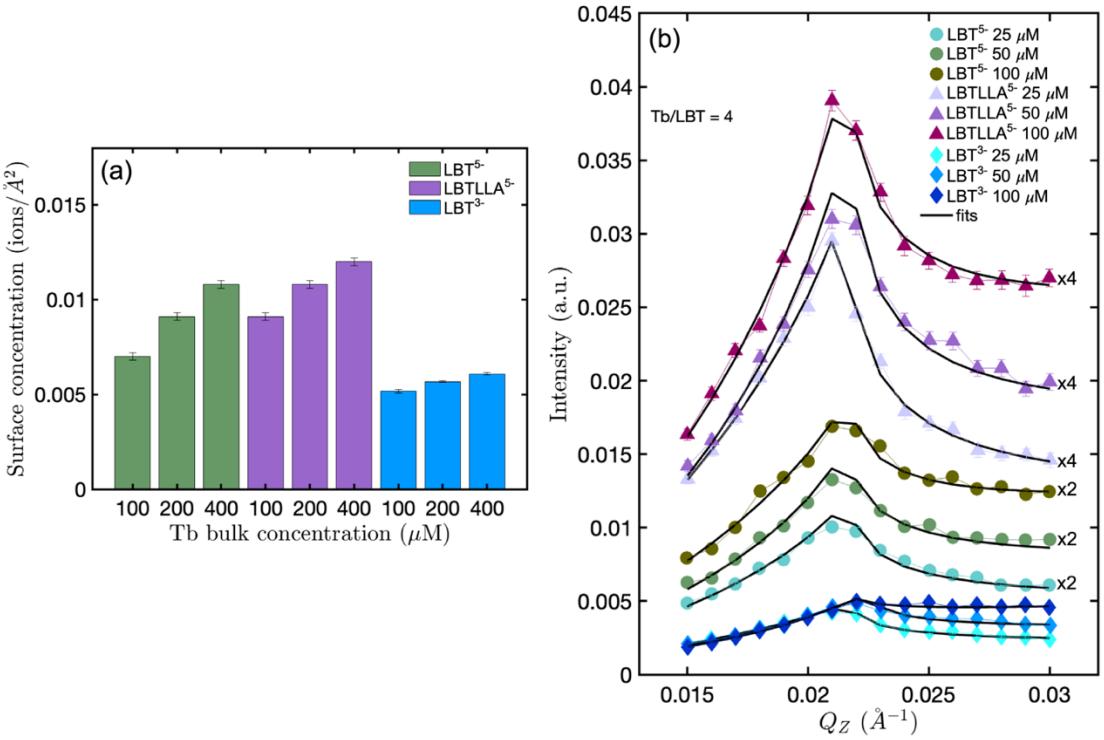

Fig. S9. (a) Terbium interfacial density as a function of peptide and cation concentration for ratios LBT:Tb^{3+} equal to 1:4. (b) Integrated terbium fluorescence intensity ($\mathcal{L}_\alpha$) as a function of Q_Z near critical angle for total reflection for different concentrations of peptide and cation.

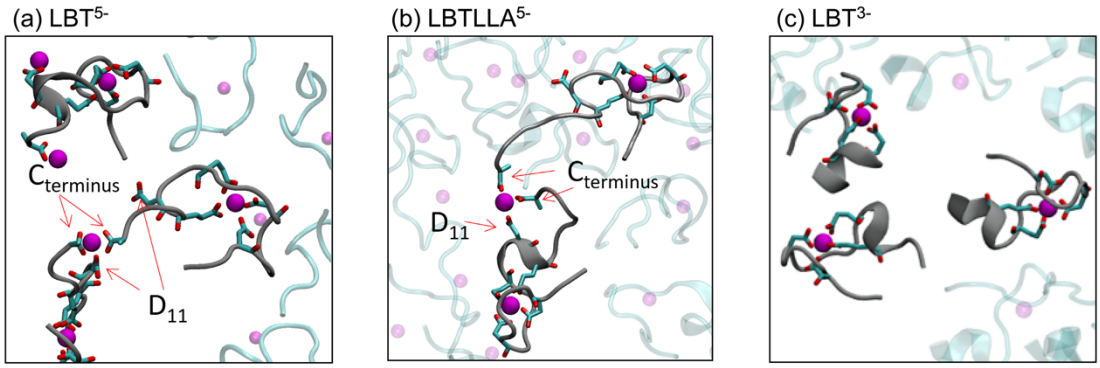

Fig. S10. Top view of instantaneous snapshots showing (a) LBT^{5-}, (b) $LBTLLA^{5-}$, and (c) LBT^{3-} peptides at the interface. A transparent representation is used for some of the adsorbed peptides and Tb^{3+} ions to aid visualization.

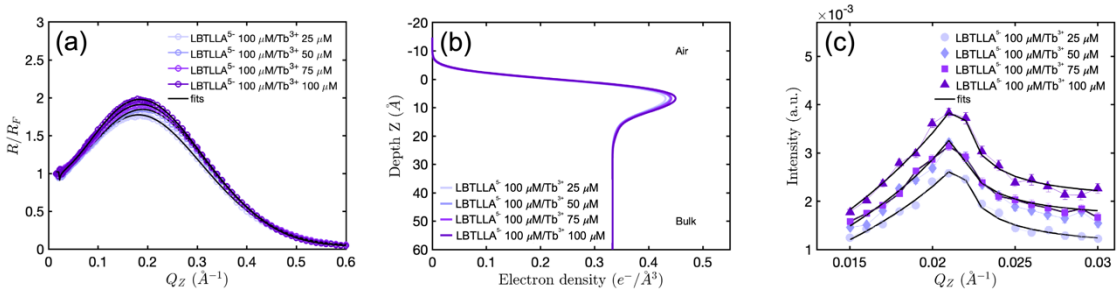

Fig. S11. (a) Normalized reflectivity ($\mathcal{R}/\mathcal{R}_{\mathcal{F}}$) as a function of Q_Z normal to the surface for layers adsorbed from solutions containing a fixed LBTLLA^{5-} peptide bulk concentration of 100 μM and different bulk Tb^{3+} concentration. Error bars, from the statistical uncertainty arising from counting photons, are plotted but are too small to be visible. (b) Electron density profiles of interfacial layers from Parratt modelling at the air/water interface for layers adsorbed from solutions containing a fixed LBTLLA^{5-} peptide bulk concentration of 100 μM and different bulk Tb^{3+} concentration. (c) Integrated terbium fluorescence intensity ($\mathcal{L}_\alpha$) as a function of Q_Z near critical angle for total reflection for layers adsorbed from solutions containing a fixed LBTLLA^{5-} peptide bulk concentration of 100 μM and different bulk Tb^{3+} concentration.

Table S3. Fitting parameters from XR measurements from adsorbed layers of solutions containing 100 μM of LBTLLA^{5-} and different concentrations of Tb^{3+}.*

	Tb^{3+} 25 μM			**Tb^{3+} 50 μM**		
Slab #	d (Å)	ρ (e^-/Å^3)	σ (Å)	d (Å)	ρ (e^-/Å^3)	σ (Å)
1	$11.31^{\pm0.09}$	$0.4418^{\pm0.0009}$	$2.93^{\pm0.01}$	$11.16^{\pm0.08}$	$0.451^{\pm0.001}$	$2.91^{\pm0.01}$
2	$7.7^{\pm0.2}$	$0.3446^{\pm0.0006}$	$2.93^{\pm0.01}$	$7.6^{\pm0.2}$	$0.3437^{\pm0.0006}$	$2.91^{\pm0.01}$
	Tb^{3+} 75 μM			**Tb^{3+} 100 μM**		
Slab #	d (Å)	ρ (e^-/Å^3)	σ (Å)	d (Å)	ρ (e^-/Å^3)	σ (Å)
1	$11.42^{\pm0.05}$	$0.4517^{\pm0.0007}$	$2.88^{\pm0.01}$	$11.33^{\pm0.05}$	$0.4625^{\pm0.0008}$	$2.97^{\pm0.01}$
2	$8.1^{\pm0.2}$	$0.3436^{\pm0.0004}$	$2.88^{\pm0.01}$	$8.7^{\pm0.1}$	$0.3446^{\pm0.0003}$	$2.97^{\pm0.01}$

*Parameters: $\boldsymbol{d}$ is the layer thickness, $\boldsymbol{\rho}$ is the density, and $\boldsymbol{\sigma}$ is the interfacial roughness. Errors in the fitted parameters are obtained by mapping the chi-squared space.

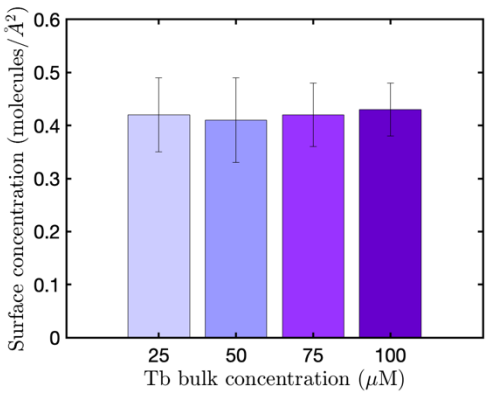

Fig. S12. Interfacial concentration of water molecules adsorbed from solutions containing a fixed LBTLLA^{5-} peptide concentration of 100 μM different bulk Tb^{3+} concentration.

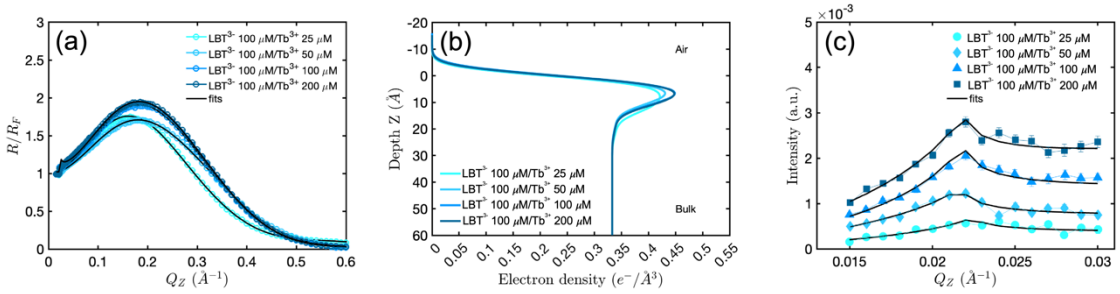

Fig. S13. (a) Normalized reflectivity ($\mathcal{R}/\mathcal{R}_{\mathcal{F}}$) as a function of Q_Z normal to the surface for interfacial layers of solutions containing a fixed LBT^{3-} peptide bulk concentration of 100 μM and different bulk Tb^{3+} concentrations. Error bars, from the statistical uncertainty arising from counting photons, are plotted but are too small to be visible. (b) Electron density profiles of interfacial layers from Parratt modelling at the air/water interface for layers adsorbed from solutions containing a fixed LBT^{3-} peptide bulk concentration of 100 μM and different bulk Tb^{3+} concentration. (c) Integrated terbium fluorescence intensity ($\mathcal{L}_\alpha$) as a function of Q_Z near critical angle for total reflection for layers adsorbed from solutions containing a fixed LBT^{3-} peptide bulk concentration of 100 μM and different bulk Tb^{3+} concentrations.

Table S4. Fitting parameters from XR measurements from adsorbed layers of solutions containing 100 μM of LBT^{3-} and different concentrations of Tb^{3+}.*

	Tb^{3+} 25 μM			**Tb^{3+} 50 μM**		
Slab #	d (Å)	ρ (e^-/Å^3)	σ (Å)	d (Å)	ρ (e^-/Å^3)	σ (Å)
1	$11.67^{\pm0.02}$	$0.4245^{\pm0.0002}$	$2.915^{\pm0.004}$	$10.7^{\pm0.1}$	$0.447^{\pm0.002}$	$3.05^{\pm0.02}$
2	$9.1^{\pm0.2}$	$0.3415^{\pm0.0002}$	$2.915^{\pm0.004}$	$10.8^{\pm0.2}$	$0.3399^{\pm0.0002}$	$3.05^{\pm0.02}$
	Tb^{3+} 100 μM			**Tb^{3+} 200 μM**		
Slab #	d (Å)	ρ (e^-/Å^3)	σ (Å)	d (Å)	ρ (e^-/Å^3)	σ (Å)
1	$10.65^{\pm0.01}$	$0.474^{\pm0.002}$	$3.26^{\pm0.04}$	$11.22^{\pm0.06}$	$0.464^{\pm0.001}$	$3.11^{\pm0.02}$
2	$10.2^{\pm0.2}$	$0.3402^{\pm0.0002}$	$3.26^{\pm0.04}$	$10.6^{\pm0.2}$	$0.3399^{\pm0.0002}$	$3.11^{\pm0.02}$

*Parameters: $\boldsymbol{d}$ is the layer thickness, $\boldsymbol{\rho}$ is the density, and $\boldsymbol{\sigma}$ is the interfacial roughness. Errors in the fitted parameters are obtained by mapping the chi-squared space.

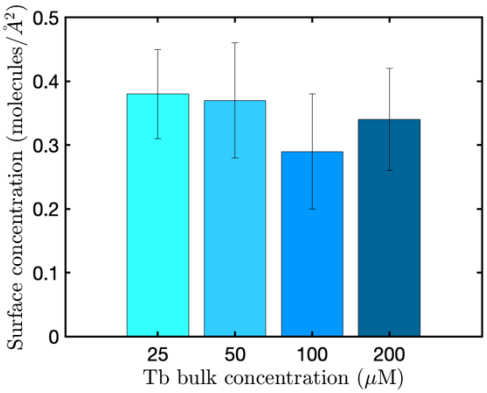

Fig. S14. Interfacial concentration of water molecules adsorbed from solutions containing a fixed LBT^{3-} peptide concentration of 100 μM and different bulk Tb^{3+} concentration.

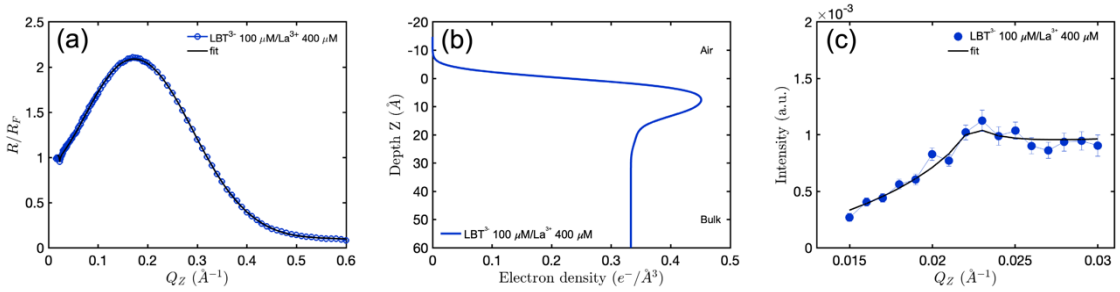

Fig. S15. (a) Normalized reflectivity ($\mathcal{R}/\mathcal{R}_{\mathcal{F}}$) as a function of Q_Z normal to the surface for interfacial layers of solutions containing 100 μM of LBT^{3-} and 400 μM of La^{3+}. Error bars, from the statistical uncertainty arising from counting photons, are plotted but are too small to be visible. (b) Electron density profiles of interfacial layers from Parratt modelling at the air/water interface for layers adsorbed from solutions containing 100 μM of LBT^{3-} and 400 μM of La^{3+}. (c) Integrated terbium fluorescence intensity ($\mathcal{L}_\alpha$) as a function of Q_Z near critical angle for total reflection for layers adsorbed from solutions containing LBT^{3-}/La^{3+} at bulk concentration of 100 μM of peptide and 400 μM of La^{3+}.

Table S5. Fitting parameters from XR measurements from adsorbed layers of solutions containing 100 μM of LBT^{3-} and 400 μM of La^{3+}.*

	LBT^{3-} 100 μM/La^{3+} 400 μM		
Slab #	$\boldsymbol{d}$ **(Å)**	**ρ** $(e^-/\text{Å}^3)$	$\boldsymbol{\sigma}$ **(Å)**
1	$13.31^{\pm 0.02}$	$0.4550^{\pm 0.0002}$	$2.913^{\pm 0.004}$
2	$9.4^{\pm 0.1}$	$0.3427^{\pm 0.0002}$	$2.913^{\pm 0.004}$

*Parameters: $\boldsymbol{d}$ is the layer thickness, **ρ** is the density, and $\boldsymbol{\sigma}$ is the interfacial roughness. Errors in the fitted parameters are obtained by mapping the chi-squared space.

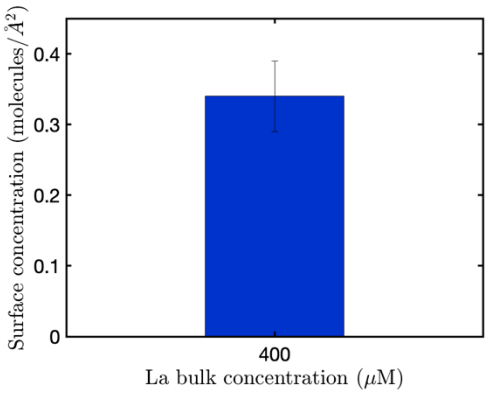

Fig. S16. Interfacial concentration of water molecules adsorbed from a solution containing 100 μM of LBT^{3-} peptide and 400 μM of La^{3+}.

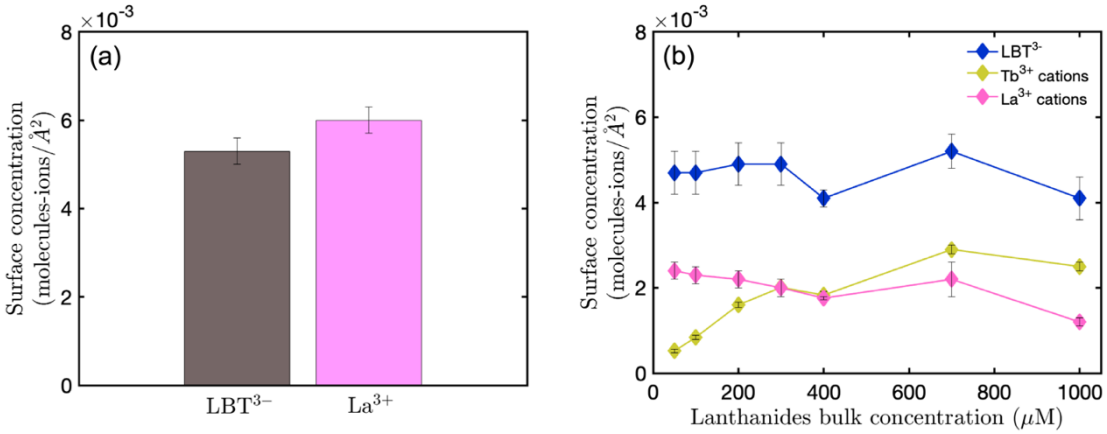

Fig. S17. (a) Interfacial concentration of LBT^{3-}, and La^{3+} cations from solutions containing 100 μM of peptide and 100 μM of cations. (b) Interfacial concentration of LBT^{3-}, Tb^{3+}, and La^{3+} for a fixed bulk concentration of peptide of 100 μM and different equimolar bulk concentrations of Ln^{3+} cations.

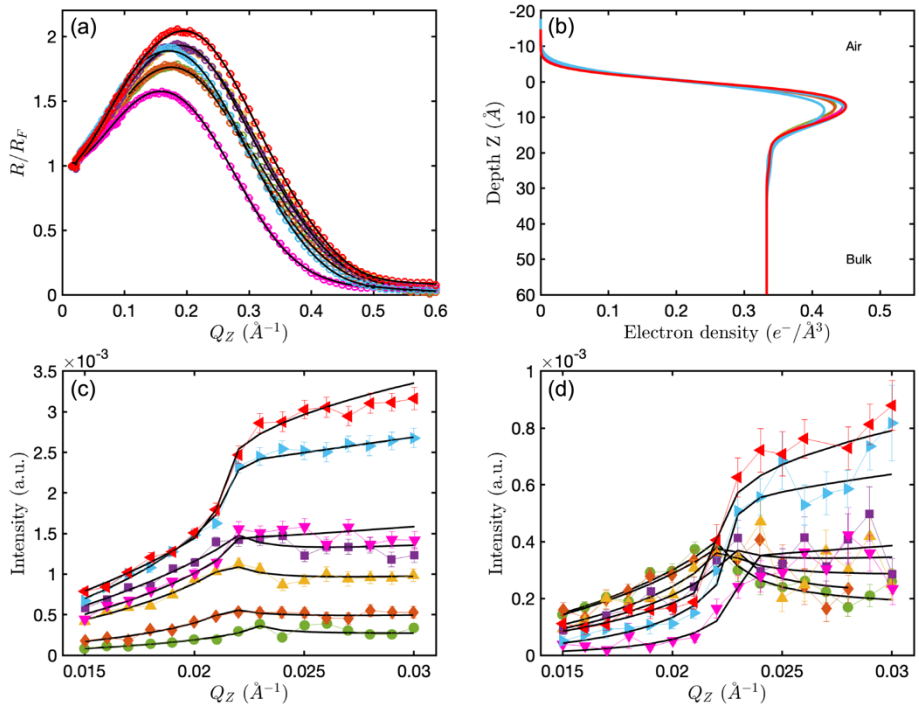

Fig. S18. (a) Normalized reflectivity ($\mathcal{R}/\mathcal{R}_{\mathcal{F}}$) as a function of Q_Z normal to the surface for interfacial layers of solutions containing $LBT^{3-}/Tb^{3+}/La^{3+}$ at a fixed peptide bulk concentration of 100 μM and different equimolar concentrations of Tb^{3+} and La^{3+}. Error bars, from the statistical uncertainty arising from counting photons, are plotted but are too small to be visible. (b) Electron density profiles of interfacial layers from Parratt modelling at the air/water interface for layers adsorbed from solutions containing $LBT^{3-}/Tb^{3+}/La^{3+}$ at a fixed peptide bulk concentration of 100 μM and different equimolar concentrations of Tb^{3+} and La^{3+}. (c) Integrated terbium fluorescence intensity ($\mathcal{L}_\alpha$) as a function of Q_Z near critical angle for total reflection for layers adsorbed from solutions containing $LBT^{3-}/Tb^{3+}/La^{3+}$ at a fixed peptide bulk concentration of 100 μM and different equimolar concentrations of Tb^{3+} and La^{3+}. (d) Integrated lanthanum fluorescence intensity ($\mathcal{L}_\alpha$) as a function of Q_Z near critical angle for total reflection for layers adsorbed from solutions containing $LBT^{3-}/Tb^{3+}/La^{3+}$ at a fixed peptide bulk concentration of 100 μM and different equimolar concentrations of Tb^{3+} and La^{3+}. Legend as follows, green: $Tb^{3+} = La^{3+} = 25$ μM, orange: $Tb^{3+} = La^{3+} = 50$ μM, yellow: $Tb^{3+} = La^{3+} = 100$ μM, purple: $Tb^{3+} = La^{3+} = 150$ μM, pink: $Tb^{3+} = La^{3+} = 200$ μM, blue: $Tb^{3+} = La^{3+} = 350$ μM, red: $Tb^{3+} = La^{3+} = 500$ μM.

Table S6. Fitting parameters from XR measurements from adsorbed layers of solutions containing of $LBT^{3-}/Tb^{3+}/La^{3+}$ at a fixed peptide bulk concentration of 100 μM and different equimolar concentrations of Tb^{3+} and La^{3+}.*

	Tb^{3+} 25 μM/La^{3+} 25 μM			**Tb^{3+} 50 μM/La^{3+} 50 μM**			**Tb^{3+} 100 μM/La^{3+} 100 μM**		
Slab #	d (Å)	ρ $(e^-/Å^3)$	σ (Å)	d (Å)	ρ $(e^-/Å^3)$	σ (Å)	d (Å)	ρ $(e^-/Å^3)$	σ (Å)
1	$11.37^{\pm0.08}$	$0.450^{\pm0.001}$	$3.16^{\pm0.02}$	$12.10^{\pm0.07}$	$0.445^{\pm0.001}$	$3.16^{\pm0.02}$	$11.60^{\pm0.05}$	$0.4574^{\pm0.0007}$	$3.02^{\pm0.01}$
2	$9.9^{\pm0.2}$	$0.3404^{\pm0.0003}$	$3.16^{\pm0.02}$	$11.8^{\pm0.3}$	$0.3338^{\pm0.0002}$	$3.16^{\pm0.02}$	$10.1^{\pm0.3}$	$0.3393^{\pm0.0002}$	$3.02^{\pm0.01}$
	Tb^{3+} 150 μM/La^{3+} 150 μM			**Tb^{3+} 200 μM/La^{3+} 200 μM**			**Tb^{3+} 350 μM/La^{3+} 350 μM**		
Slab #	d (Å)	ρ $(e^-/Å^3)$	σ (Å)	d (Å)	ρ $(e^-/Å^3)$	σ (Å)	d (Å)	ρ $(e^-/Å^3)$	σ (Å)
1	$11.80^{\pm0.04}$	$0.4576^{\pm0.0006}$	$3.06^{\pm0.01}$	$13.05^{\pm0.05}$	$0.4317^{\pm0.0007}$	$3.60^{\pm0.01}$	$12.36^{\pm0.03}$	$0.4613^{\pm0.0006}$	$3.339^{\pm0.009}$
2	$10.5^{\pm0.3}$	$0.3390^{\pm0.0002}$	$3.06^{\pm0.01}$	$14.9^{\pm0.1}$	$0.3342^{\pm0.0001}$	$3.60^{\pm0.01}$	$14.9^{\pm0.2}$	$0.3397^{\pm0.0001}$	$3.339^{\pm0.009}$
	Tb^{3+} 500 μM/La^{3+} 500 μM								
Slab #	d (Å)	ρ $(e^-/Å^3)$	σ (Å)						
1	$12.14^{\pm0.07}$	$0.457^{\pm0.001}$	$2.82^{\pm0.02}$						
2	$12.9^{\pm0.3}$	$0.3378^{\pm0.0002}$	$2.82^{\pm0.02}$						

*Parameters: d is the layer thickness, ρ is the density, and σ is the interfacial roughness. Errors in the fitted parameters are obtained by mapping the chi-squared space.

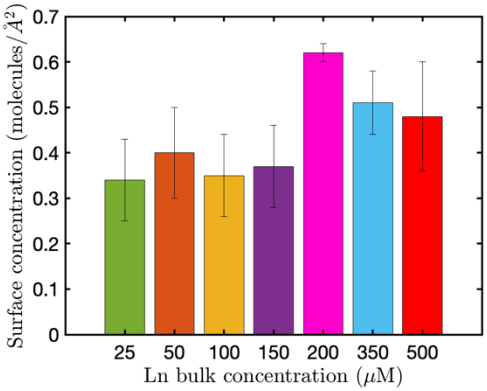

Fig. S19. Interfacial concentration of water molecules adsorbed from solutions containing a fixed LBT^{3-} peptide concentration of 100 μM and different bulk equimolar concentrations of Tb^{3+} and La^{3+}.

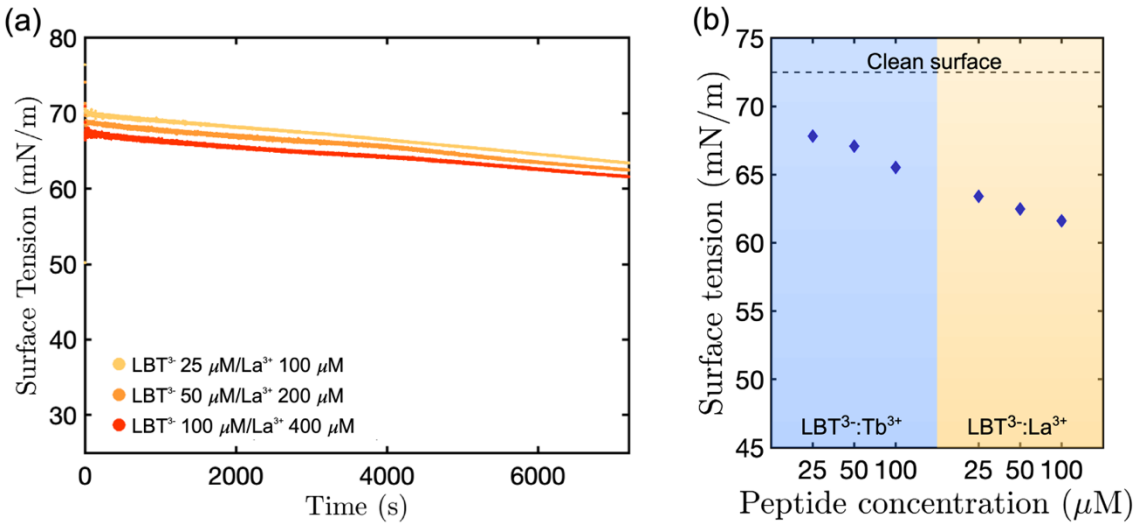

Fig. S20. (a) Dynamic surface tension relaxation measurements at different bulk concentration of LBT^{3-} peptide in the presence of La^{3+} cations at a ratio of LBT^{3-}:La^{3+} equal to 1:4. (b) Quasi-equilibrium surface tension measurements at different bulk concentration of LBT^{3-} peptide in the presence of Tb^{3+} and La^{3+} cations at a ratio of LBT^{3-}:La^{3+} equal to 1:4.

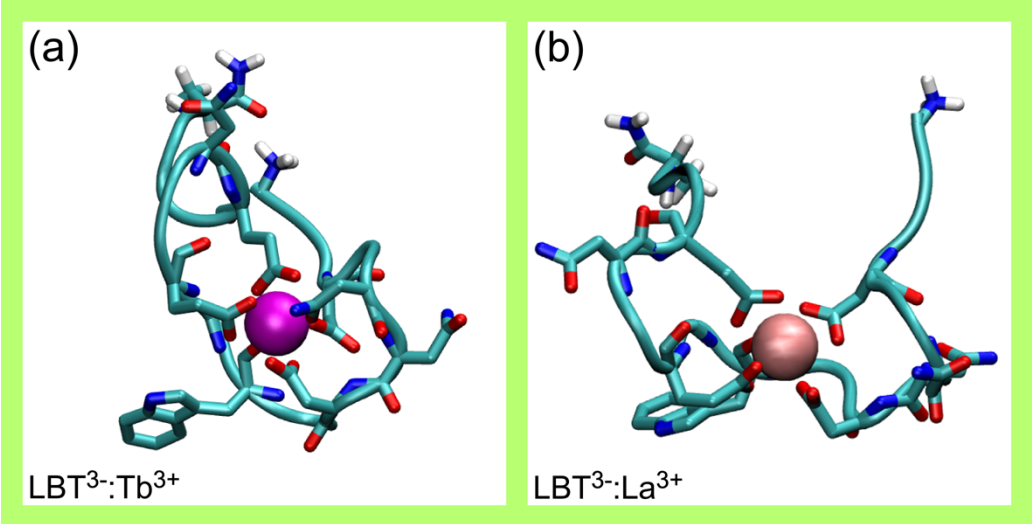

Fig. S21. MD simulation renderings of a single LBT^{3-} complex in the aqueous phase with (a) Tb^{3+} and (b) La^{3+}.

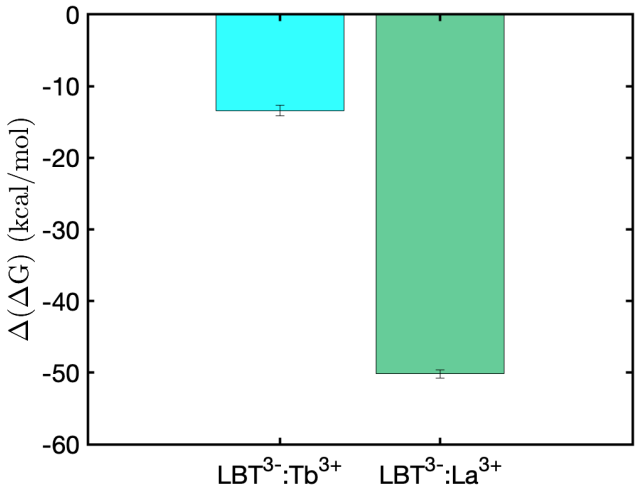

Fig. S22. Free energy of adsorption of the LBT^{3-}:Tb^{3+} and LBT^{3-}:La^{3+} complexes to the air-aqueous interface from a bulk aqueous solution.

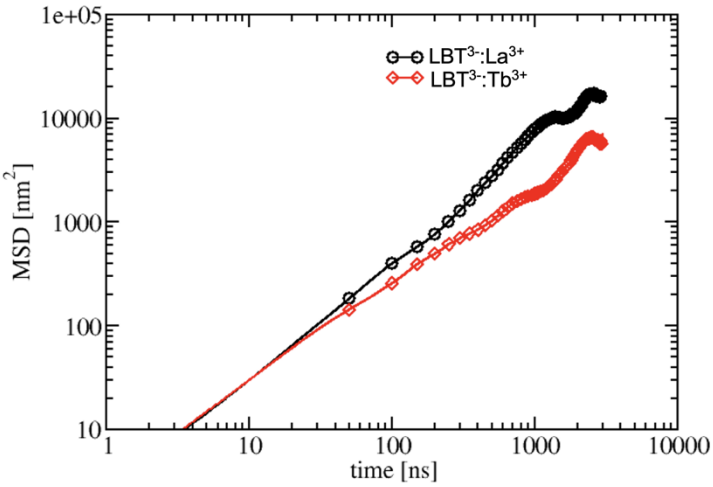

Fig. S23. Mean square displacement (MSD) averaged over 1100 ns of molecular dynamics simulations for LBT^{3-}:Tb^{3+} and LBT^{3-}:La^{3+} complexes in bulk solution.

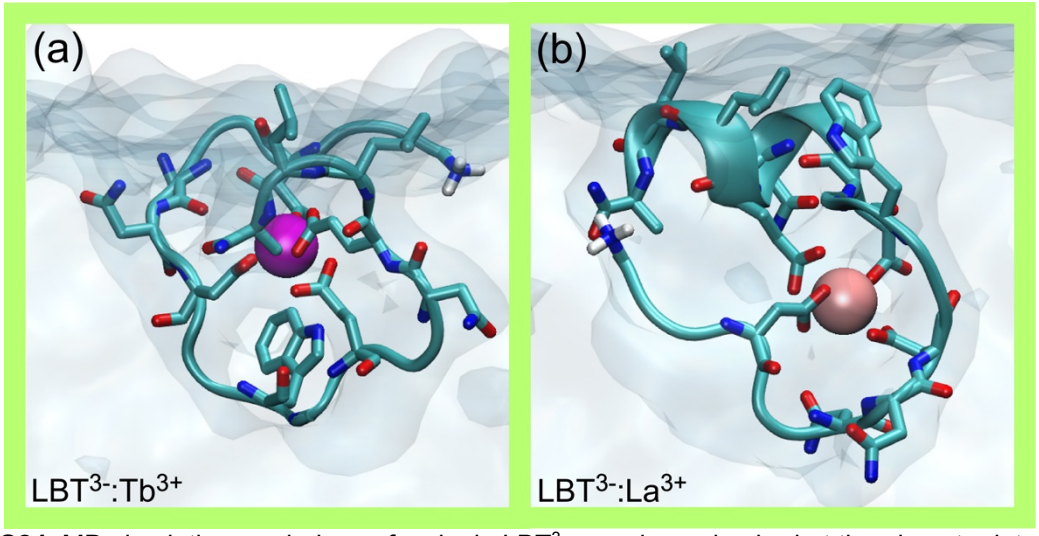

Fig. S24. MD simulation renderings of a single LBT^{3-} complex adsorbed at the air-water interface with (a) Tb^{3+} and (b) La^{3+}.

References

1. Villa, Alessandra, A. E. Mark. Calculation of the free energy of solvation for neutral analogs of amino acid side chains. *Journal of computational chemistry* 23.5, 548-553 (2002).
2. Pohorille, A., Jarzynski, C., Chipot, C. Good practices in free-energy calculations. *The Journal of Physical Chemistry B* 114, 10235–10253 (2010).
3. Christ, C. D., Mark, A. E., van Gunsteren, W. F. Basic ingredients of free energy calculations: A review. *Journal of Computational Chemistry* **31**, 1569–1582 (2010).
4. P. D'Angelo, A. Zitolo, V. Migliorati, G. Chillemi, M. Duvail, P. Vitorge, S. Abadie, R. Spezia. Revised ionic radii of lanthanoid (III) ions in aqueous solution. *Inorganic chemistry* 50, 4572-4579 (2011).
5. J. K. Grimsley, G. I. Scholtz, M. H. Pace. Hydrophobic solvation of peptides in water. *Protein Science* 18, 247–251 (2009).
6. W. Bu, M. Mihaylov, D. Amoanu, B. Lin, M. Meron, I. Kuzmenko, L. Soderholm, M. L. Schlossman. X-ray studies of interfacial strontium-extractant complexes in a model solvent extraction system. *The Journal of Physical Chemistry B* 118, 12486–12500 (2014).
7. W. Bu, H. Yu, G. Luo, M. K. Bera, B. Hou, A. Q. Schuman, B. Lin, M. Meron, I. Kuzmenko, M. R. Antonio, L. Soderholm, M. L. Schlossman. Observation of a rare earth ion-extractant complex arrested at the oil- water interface during solvent extraction. *The Journal of Physical Chemistry B* 118, 10662– 10674 (2014).